POLITECNICO DI TORINO
Repository ISTITUZIONALE

Bio-inspired non self-similar hierarchical elastic metamaterials

(Article begins on next page)

23 September 2024

Bio-inspired non self-similar hierarchical elastic metamaterials

M. Mazzotti [a], A. Foehr [b,c], O.R. Bilal [d], A. Bergamini [e], F. Bosia [f], C. Daraio [b], N.M. Pugno [g,h], M. Miniaci [a,b,e,*]

[a] *CNRS, Centrale Lille, ISEN, Univ. Lille, Univ. Valenciennes, UMR 8520 - IEMN, Avenue Henri Poincare, Villeneuve-D'Ascq, 60069, France*

[b] *Division of Engineering and Applied Science, California Institute of Technology, Pasadena, 91125, CA, USA*

[c] *Department of Mechanical and Process Engineering, ETH Zurich, Zurich, 8092, Switzerland*

[d] *Department of Mechanical Engineering, University of Connecticut, Auditorium Rd, UTEB 378, Storrs, 06269, CT, USA*

[e] *Laboratory for Acoustics/Noise Control, Empa, Überlandstrasse 129, Dubendorf, 8600, Switzerland*

[f] *Department of Applied Science and Technology, Politecnico di Torino, Corso Duca degli Abruzzi, 24, Torino, 10129, Italy*

[g] *Laboratory for Bioinspired, Bionic, Nano, Meta Materials & Mechanics, Department for Civil, Environmental and Mechanical Engineering, University of Trento, Via Mesiano 77, Trento, 38123, Italy*

[h] *School of Engineering and Materials Science, Queen Mary University of London, Mile End Road, E1, London, 4NS, United Kingdom*

ARTICLE INFO

ABSTRACT

Hierarchy provides unique opportunities for the design of advanced materials with superior properties that arise from architecture, rather than from constitutive material response. Contrary to the quasi-static regime, where the potential of hierarchy has been largely explored, its role in vibration mitigation and wave manipulation remains elusive.

So far, the majority of the studies concerning hierarchical elastic metamaterials have proposed a self-similar repetition of a specific unit cell at multiple scale levels, leading to the activation of the same bandgap mechanism at different frequencies. On the contrary, here, we show that by designing non self-similar hierarchical geometries allows us to create periodic structures supporting multiple, highly attenuative and broadband bandgaps involving (independently or simultaneously) different scattering mechanisms, namely, Bragg scattering, local resonance and/or inertial amplification, at different frequencies. The type of band gap mechanism is identified and discussed by examining the vibrational mode shapes and the imaginary component of the wavenumber in the dispersion diagram of the unit cell. We also experimentally confirm this by performing measurements in the lowest frequency regime on a 3D printed structure.

Hierarchical design strategies may find application in vibration mitigation for civil, aerospace and mechanical engineering.

1. Introduction

In Nature, complex structural designs have emerged from millions of years of evolution and adaptation of organisms to their living environment [1,2]. This has led to structural architectures with optimized mechanical properties like strength, toughness and damage resilience, widely observed in many natural materials like wood, bone, spider silk or sponges [3–6]. A common feature responsible for these exceptional properties is a hierarchical organization of the structure deriving from a functional adaptation at different scale levels, through growth and re-modelling [7]. Therefore, structural hierarchy [8,9] has emerged as one of the main characteristics pursued in bioinspired research. The recent advances in three-dimensional macro- [10], micro- [11] and nano-fabrication [12,13] have boosted this research field even further,

offering unprecedented possibilities to realize advanced structured materials [14] for engineering applications, also strongly impacting the field of elastic and acoustic metamaterials [15–17], which are materials that derive their unusual dynamic response from the geometry of their structure rather than from the mechanical properties of their constituent materials.

In the quasi-static loading regime, hierarchy in material structures has been studied extensively and has been shown to convey extreme damage tolerance [18], extraordinary deformation recoverability [19], simultaneous exceptional lightness and stiffness [20], and efficient energy dissipation mechanisms [21,22]. More recently, Yin et al. investigated the effects of architecture levels on the mechanical properties of hierarchical lattice materials. Designing hybrid-type hierarchical lattice

---

materials with different architectures, they discussed the effects of macroscopic and mesoscopic configurations, deducing a generalized analytical model of nth order lattices [23]. Wang et al. investigated the compression behaviour of strut-reinforced hierarchical lattices through experiments and simulations, parametrically determining the effects of the geometry and discussing the relation between the master-cell and slave-cell [24].

On the contrary, in wave propagation problems, the effect of hierarchical designs has been less explored, especially in the field of elastic and acoustic metamaterials [25]. Zhang and To were amongst the pioneers in introducing a representative unit cell repeated in a self-similar manner at various length scales. In this work, the considered unit cell included two materials (a very stiff one and a very compliant one) and it was found that the introduction of the structural hierarchy allowed to open additional BGs at multi-scale frequencies [26]. Miniaci et al. reported a similar effect in hierarchical phononic crystals made of a single material [27,28]. More recently, Jiang et al. proposed multifunctional metamaterials possessing both vibration mitigation and energy absorption properties. They observed low-frequency local resonance bandgaps in lightweight lattice structures and showed that a functionally graded strategy could enhance such multifunctional performance [29]. Gao et al. observed large bandgaps in two-dimensional phononic crystals with fractal structure [30] and characterized by self-similarity [31,32]. They observed that the introduction of fractality and self-similarity in phononic crystals may lead to a change of the number, of the location and of the width of the bandgaps.

To date, elastic and acoustic metamaterials have been designed to exploit three main distinct mechanisms for the control of wave propagation: (i) the Bragg scattering mechanism [33–35], (ii) local resonances [36], and/or (iii) inertial amplification [37–39]. Although based on scattering induced by different mechanisms, these approaches all allow to achieve unusual dynamic behaviour, including (but not limited to) nonreciprocal and scattering-free wave propagation [40,41], cloaking [42,43] and frequency bandgaps – BGs [44].

Bragg scattering arises in periodically arranged unit cells, and requires the wavelength of the incoming waves to be comparable to the structural periodicity of the material. When targeting low BG frequency ranges, this requirement inevitably leads to large unit cell sizes.

Locally resonant structures [45–49], instead, decouple the frequency at which a BG is opened from the size of the unit cell [50], as they derive their dynamic behaviour from the eigenfrequencies of the resonators rather than the periodicity of the structure. The main drawback of this approach is that resonating behaviours usually produce narrow frequency BGs, often requiring heavy masses [36] or very compliant structures [48].

Inertial amplification reduces the need for heavy masses, and exploits displacement mechanisms to amplify the effective inertia of specific regions of the unit cell [51–54], with, however, the main drawback of a significant reduction of the structural stiffness [55]. Nevertheless, inertial amplification allows to attain sub-wavelength and broadband BGs, in lightweight structures [38].

Previous work has explored the use of these mechanisms individually, leading to unit cell designs optimized with respect to specific BG nucleation mechanism [56,57]. A limited number of studies has addressed the interaction of BGs deriving from Bragg scattering and local resonances [58,59], with the proposal of multi-material structures [60–62] or even single-material architectures [63,64]. For instance, Xiao et al. observed and discussed the formation of a wide bandgap due to the exact coupling between Bragg and resonance gaps in a uniform string with periodically attached mass–spring resonators. The formation of the bandgap was discussed through an analytical model with explicit formulations [65]. Tian et al. merged Bragg and local resonance bandgaps in perforated elastic metamaterials with embedded spiral holes [66]. Li et al. investigated a meta-beam for three-directional broadband vibration suppression and, coupling local resonances and Bragg scattering, observed a four fold enlargement of the attenuation

bandwidth with respect to the conventional design [67]. Frandsen et al. investigated the possibility to couple Bragg scattering and inertial amplification mechanisms by investigating the wave motion in a continuous elastic rod with a periodically attached mechanism exhibiting properties similar to those of an "inerter" typically used in vehicle suspensions [68]. Similarly, Mi and Yu observed an improved sound insulation performance from a new type of acoustic metamaterial, built by attaching a periodic triangular bar-and-hinge device to a host beam [69].

However, a strategy encompassing all three scattering mechanisms (Bragg scattering, local resonance and inertial amplification mechanism) remains unexplored, so far.

Here, we show that introducing the concept of hierarchy in elastic metamaterials naturally leads to the realization of a new class of periodic structures, capable of generating multiple, highly attenuative and broadband BGs at multi-scale frequencies, including the most challenging deep sub-wavelength regime. The approach also allows to deal with a single-material, and thus easy-to-manufacture (and recycle), structures, favouring lightweight designs. Hierarchy is here understood in the sense that the representative unit cell of the periodic structure may comprise multiple arrangements of non self-similar inhomogeneities at various length scales. Specifically, the unit cell is realized by introducing, in a continuous matrix, cross-like cavities, which have been shown to provide an optimal geometry to activate various types of scattering mechanisms at different length scales [51,70,71].

In wave dynamics, two main approaches exist to introduce a hierarchical organization in elastic metamaterials. The first involves the use of lattice-type architectures, consisting for instance of beam-like structures periodically arranged over multiple scale levels [72,73]. These structures lead to enhanced dynamic properties in terms of BG opening, as well as advanced load-bearing [74] or thermal insulation capabilities [75]. A second approach seeks to achieve broadband vibration mitigation at multiple frequency scales by introducing hierarchy into continuous structures. In this context, both multi-material [26] and single-material [27] systems have been explored, finding advantages such as the nucleation of additional hierarchically induced BGs in the mid-frequency range and the shift of BGs to lower frequencies due to the mass-to-stiffness ratio change, controlled by a "hierarchical factor" (i.e., the length scaling parameter between geometries in a hierarchical structure) [27].

However, up to now, the BG nucleation mechanism invoked by these approaches have always involved the same physical mechanism (for instance, Bragg scattering due to the scalability of the wave equation [27] or local resonances [26]), activated at different frequency scales. This is a direct consequence of adopting the assumption of strong self-similarity, implying a down- (or up-) scaling of the same unit cell in a recursive manner, when proceeding from a hierarchical level to the other.

Here, we remove the assumption of strict self-similarity and conceive a hierarchical non self-similar metamaterial (see Fig. 1a) encompassing all the main known scattering mechanisms (Bragg scattering, local resonance and inertial amplification) into a single unit cell. This also allows to generate a hierarchical design that is closer to natural structures, which can include elements of periodicity, but not necessarily of self-similarity [1,76–78].

A schematic representation of the fabricated unit cell used in this study is shown in Figs. 1b–d. It includes two hierarchical levels, consisting of cross-like cavities introduced at different length scales, in a continuous thermoplastic polymer matrix (Figs. 1b–c). At each hierarchical level, the added cross-like cavities are selectively scaled-down and appropriately stretched to fit in the mass- and connecting-regions of the previous hierarchical level (Fig. 1b). The design strategy, here implemented for only two hierarchical levels, can be recursively extended to n hierarchical levels.

The inclusions have been chosen in the shape of cross-like cavities due to their effectiveness in activating different types of scattering
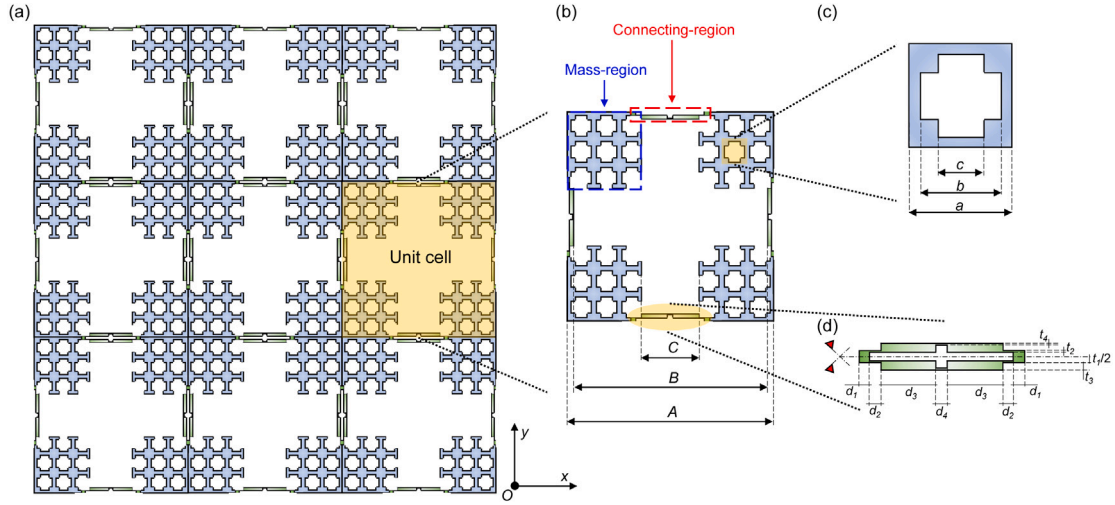
Fig. 1. Design strategy of the non-self-similar hierarchical metamaterial. (a) In-plane view of the finite hierarchical elastic metamaterial under investigation made of 3×3 unit cells. The single unit cell is highlighted by the light orange shading. (b) Schematic representation of the single hierarchical unit cell allowing to control the wave propagation at multiple frequency scales by activating multiple BG mechanisms (inertial amplification, Bragg scattering and local resonance). The unit cell is here organized over two hierarchical levels, and obtained by opening cross-like holes into a continuous thermoplastic polymer Acrylonitrile Butadiene Styrene (ABS) matrix at different length scales. (c, d) Cross-like holes are selectively stretched, so as to fit different regions of the unit cell, named mass- and connecting-regions, respectively. Relaxing the requirement of self-similarity in the introduction of hierarchy allows the activation of inertial amplification, medium and high frequency Bragg scattering mechanisms, as well as local resonances. The design strategy, realized in this work for only two hierarchical levels, can be recursively extended to n levels, according to the adopted scheme. Geometrical parameters of the unit cell are provided in Tables 1 and 2.

mechanisms [39,51,70]. The elongation of the connecting regions of the cross-like cavities from a hierarchical level to the next allows the realization of a single unit cell capable of triggering at the same time: (1) inertial amplification (Fig. 1d), (2) medium (Fig. 1b without the small cross-like cavities) and high (Fig. 1c) frequency Bragg scattering, as well as (3) several local resonances. The novelty of this study lies in the simultaneous combination of these three mechanisms.

2. Mathematical modelling

In this section, we report the mathematical framework and the computational approach used to calculate the dispersion curves of the considered structures.

In the case of wave propagation in a homogeneous, isotropic and linear elastic material, the following equations of motion holds:

$$\frac{E}{2(1+\nu)(1-2\nu)} \nabla(\nabla \cdot \mathbf{u}) + \frac{E}{2(1+\nu)} \nabla^2 \mathbf{u} = -\rho \omega^2 \mathbf{u} \tag{1}$$

where $\mathbf{u} = \mathbf{u}(\mathbf{r})$ is the displacement vector, $\mathbf{r}$ the position vector and $\omega = 2\pi f$ the angular frequency. E, ν and ρ denote the Young's modulus, the Poisson's ratio and the mass density of the material composing the unit cell, respectively.

Dispersion curves are computed via the Finite Element solver COM-SOL Multiphysics by using the Bloch–Floquet theory, i.e., implementing the periodic boundary conditions at the edges of the unit cells, $\mathbf{u}_{\mathrm{dst}} = \mathbf{u}_{\mathrm{src}} \cdot e^{-i\mathbf{k}^* \cdot (\mathbf{r}_{\mathrm{dst}} - \mathbf{r}_{\mathrm{src}})}$, with $\mathbf{k}^*$ the reduced Bloch wavevector, and the subscripts dst and src indicating the destination and source nodes of the domain where the periodic boundary conditions are applied, respectively.

Dispersion curves are calculated considering the unit cell infinitely duplicated in a square array (or a linear array for the case of the solely inertial amplification-based unit cell, i.e., the one reported in Fig. 1d). The out-of-plane dimension of the unit cells is assumed to be sufficiently large to allow for a 2D plane-strain approximation to be adopted, i.e., dispersion bands are calculated for in-plane modes only. A linear elastic constitutive law is adopted and the following mechanical parameters are used for the material: density $\rho = 1170 \ \mathrm{kg/m}^3$, Young's modulus $E = 2$ GPa, and Poisson's ratio $\nu = 0.35$ [79]. Domains are meshed by means of 4-node quadrilateral elements of maximum size

$L_{FE} = 20 \ \mu\mathrm{m}$, which is found to provide accurate eigensolutions up to the frequency of interest.

The resulting eigenvalue problem $(\mathbf{K} - \omega^2\mathbf{M})\mathbf{u} = \mathbf{0}$ is solved by: (i) varying the non-dimensional wavevector $\mathbf{k}^*$ (allowing to obtain the real component of the reduced wavenumber); (ii) varying the frequency and deriving the wavenumber (allow to extract the imaginary part of the wavenumber [80,81]).

3. Results

To verify that the proposed non self-similar hierarchical unit cell supports multiple scattering mechanisms, in this section we first numerically calculate its dispersion diagram and mode shapes and compare them with those of the corresponding non hierarchical structures. Then, we measure the frequency response function (FRF) of a 3×3 unit cell sample finding a good agreement with the numerical predictions.

The central panel of Fig. 2 reports a schematic representation (in semi-logarithmic scale) of the overall behaviour achieved by the non self-similar hierarchical elastic metamaterial (HEM) from few Hz to tens of kHz. For the sake of clarity, the dispersion curves are not reported explicitly but substituted by white and light blue rectangles corresponding to: (i) mainly propagative and (ii) mainly attenuative regions, respectively. Zooms of the dispersion curves in specific frequency regions are also provided. In addition, illustrative mode shapes reported in the figure unequivocally show how at different frequency scales distinct mechanisms are activated, involving deformation of different parts of the unit cell. For instance, at the lowest frequencies (0–1100 Hz), the inertial amplification mechanism is activated in the connecting-regions, and is the main driver for the BG opening, whereas in the mid frequency range (1100–4400 Hz) it can be seen that the whole structure contributes to the BG, and finally in the highest frequency range (28–37 kHz), mainly the smallest cross-like cavities deform. Mode shapes are reported as a function of the von Mises stress σ_{vM} normalized with respect to its maximum value (colours report the stress levels in the unit cells, varying from the zero stress condition – blue - to the maximum stress condition – red). The mode shapes are taken at specific values of $\mathbf{k}^*$, corresponding to the abscissae of the marker used to identify the mode shape. More precisely, at the Γ point of the first irreducible Brillouin zone for the 0–1100 Hz frequency range (star-like marker)
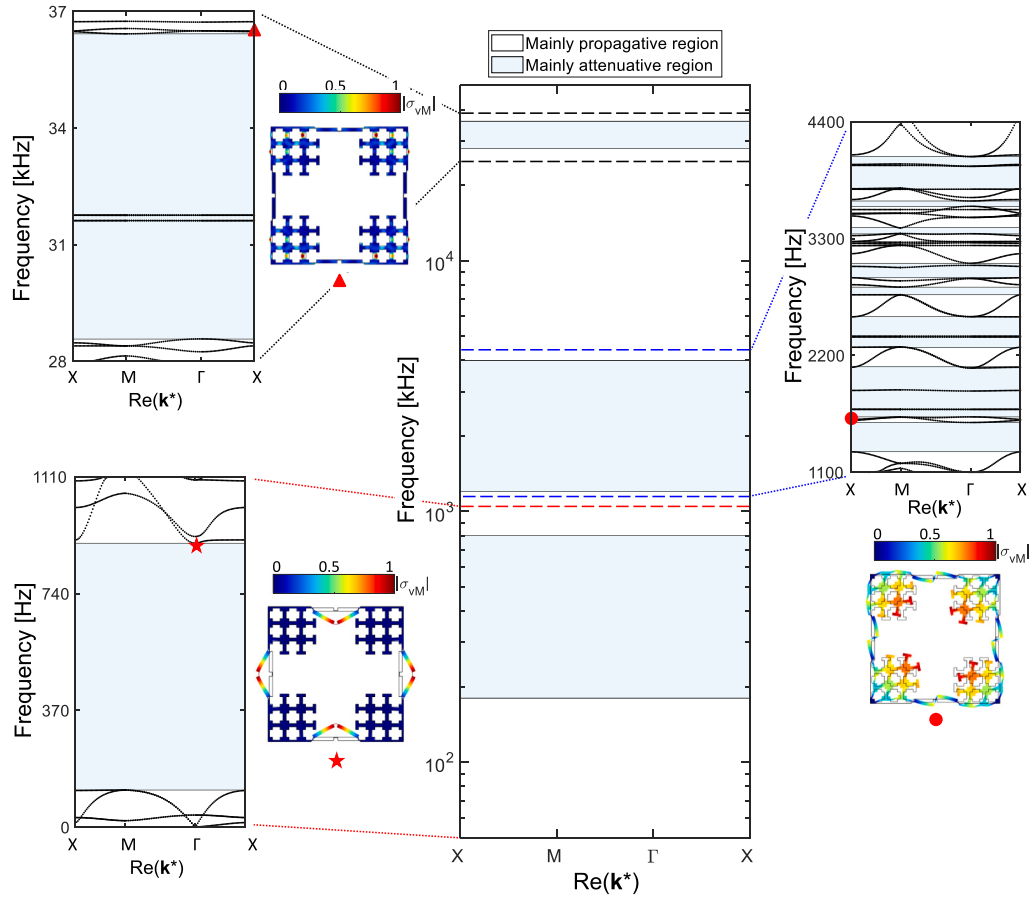
Fig. 2. Dispersion diagram of the hierarchical elastic metamaterial spanning multiple frequency scales and selectively activating deformation concerning different unit cell regions. A schematic representation of the whole dispersion diagram (from few Hz to tens of kHz) of the hierarchical elastic metamaterial is shown in the central panel. For the sake of visualization, the y-axis of the diagram has been reported in log-scale. The diagram has been divided into (i) mainly propagative regions and (ii) mainly attenuative regions, indicated by white and light blue rectangles, respectively. Magnifications of specific frequency regions are provided along with an illustrative mode shape showing how at different frequency scales distinct mechanisms are activated, both partially or wholly involving the unit cell deformation. For instance, at the lowest frequencies (0–1100 Hz), the inertial amplification mechanism is activated in the connecting-regions, and is the main responsible for the BG opening, whereas in the mid frequency range (1100–4400 Hz) it emerges that the whole structure contributes to the BG, and finally in the highest frequency range (28–37 kHz), mainly the smallest cross-like cavities deform. Mode shapes are reported including a colour map representing the von Mises stress σ_{vM} normalized to its maximum value. The mode shapes are taken at specific values of $\mathbf{k}^*$, corresponding to the abscissa of the marker used to identify the mode shape: at the Γ point of the first irreducible Brillouin zone for the mode shape between 0–1100 Hz frequency range (star-like marker) and at the X point for the other two mode shapes (triangular and circular markers).

and the X point for the other two mode shapes (triangular and circular markers).

To gain further insight about the nature of the mechanisms opening the BGs, dispersion curves of the HEM are investigated in the low, mid and high frequency regimes, and compared to the corresponding diagrams for the non-hierarchical unit cells.

Fig. 3a compares the dispersion curves in the lowest frequency regime, 0–1100 Hz, for the HEM (left panel) and the solely inertial amplification-based unit cell (right panel) reported in Fig. 1b and Fig. 1d, respectively. The diagrams present the real part of the reduced wavenumber $\mathbf{k}^*$ along the $X – M – \Gamma – X$ boundary of the first irreducible Brillouin zone (left part of the diagram) in black, as well as its imaginary component along the $\Gamma – X$ path (right part of the diagram) in red. The size of the inertial amplification mechanism is kept constant in the two structures, in order to quantify the effects of the introduction of hierarchy on the wave dispersion in the same frequency range. A direct comparison of the diagrams (real component of the reduced wavenumber) reveals that hierarchical organization allows an overall enlargement of the BG in the lower frequency regime, given by the fusion of the two BGs generated by the non-hierarchical inertial amplification-based unit cell. This is achieved through a substantial down-shift of the branch occupying the mid frequencies of the non-hierarchical structure, highlighted in green in Fig. 3a. The curve shift

is due to a change in the position of the virtual hinges of the mechanism introduced by the hierarchy.

Despite locally changing the dispersion diagram for specific branches, the introduction of hierarchy does not affect the overall dynamics of the structure, in the sense that apart from a small frequency down-shift of the dispersion curves (due to the stiffness change of the connecting-regions), the inertial amplification mechanism, responsible for the BG nucleation at such low frequencies, can freely take place in the connecting regions of the HEM. This is clearly shown in Fig. 3b, where the mode shapes at the high symmetry point X are presented for both the HEM unit cell (M1/M2), and for the solely inertial amplification-based unit cell (m1/m2). In other words, hierarchy allows the introduction of an additional degree of freedom for band manipulation and nucleation of BGs.

The vibrational behaviour in the mid (1100–4400 Hz) and high (28–37 kHz) frequency regimes of the HEM derives from the contribution of the dispersion diagrams of the corresponding non-hierarchical unit cells, i.e., the ones reported in Figs. 1c,d and that in Fig. 1b without the small cross-like cavities.

In the case of the mid frequency regime (Fig. 4a), it is possible to observe two main effects produced by the introduction of hierarchy: (i) a partial conservation of the non-hierarchical BG, and (ii) a small global down-shift of its frequencies. The BG is partially preserved, in
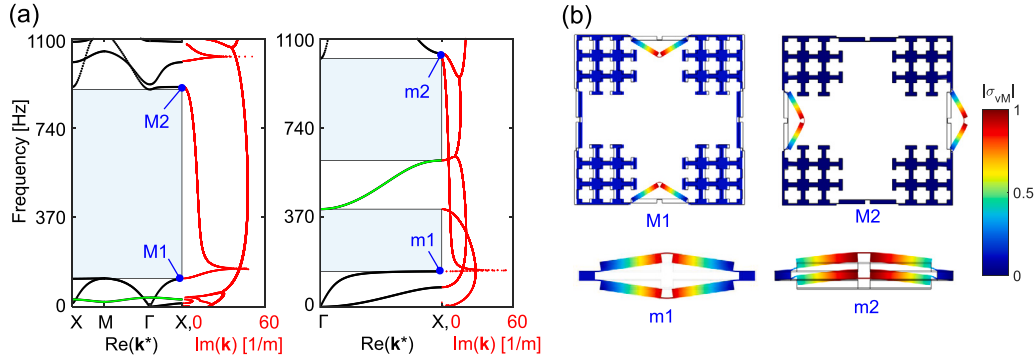
Fig. 3. Dispersion diagrams and mode shapes in the low frequency regime. (a) Dispersion curves for the hierarchical elastic metamaterial (left panel) reported in Fig. 1a, and the solely inertial amplification-based unit cell (right panel) reported in Fig. 1d. The diagrams report the real part of the reduced wavenumber Re($\mathbf{k}^*$) along the X−M−Γ−X irreducible path (left part of the diagram) in black, as well as the imaginary part of the wavenumber Im($\mathbf{k}$) along the Γ − X direction (right part of the diagram) in red, in the 0–1100 Hz frequency range. The band structures are computed considering the unit cell as infinitely replicated in a square and linear arrays for the hierarchical elastic metamaterial and solely inertial amplification-based unit cell case, respectively. In both cases, only in-plane modes are considered. From the comparison, the superior performance of the hierarchical elastic metamaterial in terms of low frequency attenuation clearly emerges as a unique larger (from 117 Hz to 900 Hz) and more efficient (larger values of the imaginary part of the wavenumber) BG, highlighted as a light blue rectangle. This effect is due to the introduction of hierarchy which introduces an important shift towards lower frequencies of the branch highlighted in green. (b) Mode shapes at the high symmetry point X: M1 and M2 denote the two mode shapes at the edge of the BG for the hierarchical elastic metamaterial, while m1 and m2 indicate modes referring to the solely inertial amplification-based unit cell. The comparison shows how the introduction of hierarchy does not affect the overall dynamics (apart from a slight frequency down-shift due to the stiffness change of the connecting-regions of the inertial amplification mechanism responsible for the BG opening). The von Mises stress distribution σ_{vM} normalized to its maximum value is shown along with modal shapes.
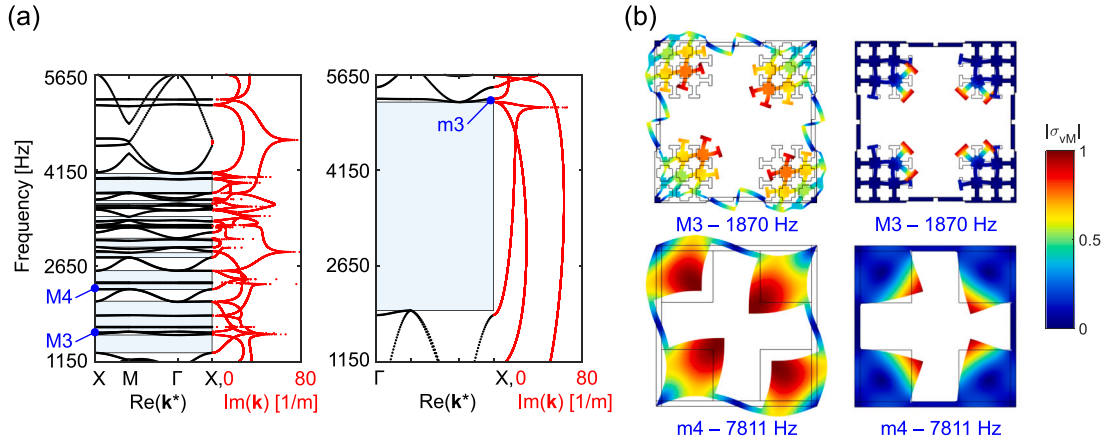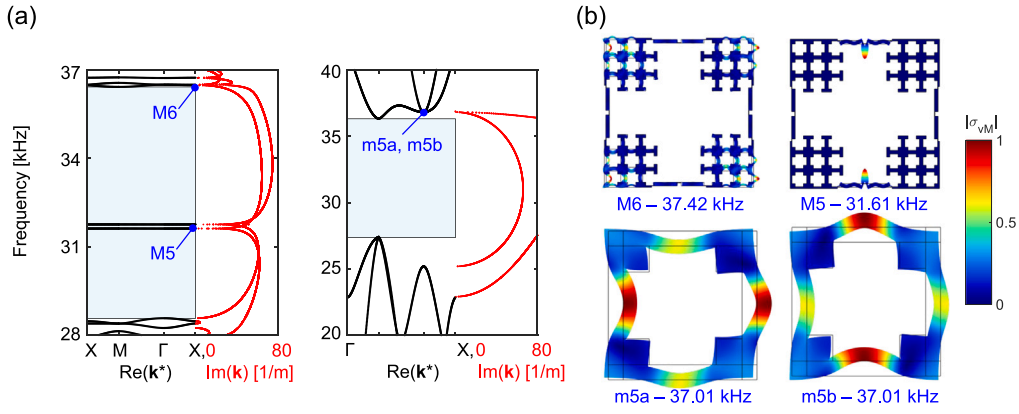

Fig. 4. Dispersion diagrams and mode shapes in the mid frequency regime. (a) Dispersion curves for the hierarchical elastic metamaterial (left panel) reported in Fig. 1a and the corresponding unit cell made of a single big cross-like cavity (right panel). The diagrams report the real part of the reduced wavenumber Re($\mathbf{k}^*$) along the X − M − Γ − X irreducible path (left part of the diagram) in black, as well as the imaginary part of the wavenumber Im($\mathbf{k}$) along the Γ − X direction (right part of the diagram) in red. A partial conservation of the non-hierarchical BG and a slight global down-shift of its frequencies are the two main effects deriving from the introduction of the hierarchy. The imaginary part of the diagrams reveals the activation of multiple mechanisms (including Bragg scattering and local resonances) in the hierarchical elastic metamaterial, and a Bragg-like scattering behaviour in the case of the corresponding non-hierarchical unit cell made of a single big cross-like cavity. In all the calculations, the band structures are computed considering the unit cells infinitely replicated in square arrays. (b) The reconstruction of the mode shapes highlights the preservation of the global deformation mechanisms (*cf* mode shapes M3/M4 and m3/m4). Mode shapes are reported as a function of the von Mises stress σ_{vM} normalized to its maximum value.

the sense that some of the pre-existing dispersion curves are altered due to a change of the stiffness-to-mass ratio in the HEM. As a consequence, new curves are introduced, the majority of which, however, correspond to localized modes, i.e., they exhibit a flat behaviour with respect to the frequency. The stiffness-to-mass ratio alterations produce a BG down-shift – from 1900–5170 Hz in the case of the non-hierarchical unit cell (right panel of Fig. 4a), to 1280–4072 Hz in the hierarchical one. Interestingly, despite this variation, hierarchy allows to preserve the global deformation mechanisms of the previous hierarchical levels (compare mode shapes M3/M4 and m3/m4 in Fig. 4b).

Analysis of the imaginary component of the wavenumber in the diagrams reveals that the introduction of hierarchy activates multiple attenuation mechanisms, including both Bragg scattering and local resonances. Indeed, we know that (i) the attenuation of the energy transmitted at a given frequency is given by the curve with the smallest value of Im($\mathbf{k}$) and that (ii) a parabolic behaviour of the attenuation curve indicates a Bragg scattering mechanism, whereas sharp spikes

indicate the presence of local resonances. Now, when the lowest value of attenuation always belongs to the same curve (as for example in Fig. 5a), only one mechanism takes place (Bragg scattering in this case). On the contrary, when two curves of different nature cross, such as for instance in Fig. 3a or Fig. 4a, coupling takes place. This confirms the suggested idea that hierarchy can be seen as a means to introduce additional degrees of freedom into the unit cell, especially if the requirements for strict self-similarity are relaxed.

There is a different relation between the vibration behaviour of HEM and of the unit cell with cross-like cavities reported in Fig. 1c. Comparing their band diagrams (Fig. 5a) we can observe that: (i) a total BG conservation occurs (apart from a couple of localized modes, such as the one indicated as M5 in Fig. 5b), and (ii) no BG shift in frequency is observed. This is due to the fact that the unit cell with cross-like cavities reported in Fig. 1c is the last hierarchical level, and is thus the main structure responsible for the determination of the BG properties of the whole unit cell at the highest frequencies. In this case, apart from

Fig. 5. Dispersion diagrams and mode shapes in the high frequency regime. (a) Dispersion curves for the hierarchical elastic metamaterial (left panel) reported in Fig. 1a and the non-hierarchical unit cell (right panel) reported in 1C. Since the non-hierarchical unit cell with the cross-like hole represents the last hierarchical level, total BG conservation occurs (apart from a couple of localized modes, such as the one named M5) and no BG shift in frequency is observable. The comparison of the imaginary component of the wavenumber reveals that the attenuating performance is not altered by the introduction of the hierarchy for the vast majority of frequencies. In all the calculations, the band structures are computed considering the unit cells infinitely replicated in bi-periodic square arrays. (b) At the edge of the BGs, the deformation mechanisms of the non-hierarchical unit cell (m5a/m5b) are mostly unaltered in the hierarchical elastic metamaterial unit cell (M6). Mode shapes are reported including a colour map representing the von Mises stress σ_{vM} normalized to its maximum value.

Table 1
Geometrical parameters of the solely inertial amplification-based unit cell presented in Fig. 1d. Parameters are given as a function of t_2, which is reported in [μm].

t_1	t_2	t_3	t_4	d_1	d_2	d_3	d_4
$8t_2$	384	$8t_2$	t_2	$13t_2$	$5t_2$	$50t_2$	$10t_2$

Table 2
Geometrical parameters of the unit cells presented in Fig. 1b,c. Parameters are given as a function of t_1 and t_2, reported in the previous table (Table 1).

A	B	C	a	b	c
$3280t_2$	$0.935A$	$0.290A$	$5t_1$	$0.800a$	$0.450a$

the modes located around 31.6 kHz, the wave attenuation performance is not altered by the introduction of hierarchy for the vast majority of frequencies concerned by the BG, but in proximity of these localized modes, where Im(**k**) rapidly goes to zero. For the same reason, at the edge of the BGs, the deformation mechanisms of the non-hierarchical unit cell (m5a and m5b in Fig. 5b) are reproduced mostly unaltered in the HEM unit cell (M6 in Fig. 5b).

We validate our approach performing experiments in the low frequency regime. We manufacture a HEM sample, such as the one shown in Fig. 6a, via additive manufacturing. The specimen consists of 3×3 unit cells. The chosen material is the thermoplastic polymer Acrylonitrile Butadiene Styrene (ABS), with the following nominal properties: density $\rho = 1170$ kg/m^3, Young's modulus $E = 2$ GPa, and Poisson's ratio $\nu = 0.35$ [79]. The geometrical parameters are listed in Tables 1 and 2. Elastic waves are excited through a mechanical shaker solidly attached to the structure through a screw and used to generate elastic waves through a frequency sweep ranging from 50 Hz to 1100 Hz (Fig. 6a).

Figs. 6b,c show in-plane magnifications of the mass- and connecting-regions of the HEM, respectively. The most critical part to print included regions of only 0.384 mm in width (corresponding to the hinges of the inertial amplification mechanism).

The transmissibility of the system, calculated as the ratio of the detected velocity in the x-direction (averaged over the four cyan points reported in Fig. 6a) and the imposed velocity at the shaker, is investigated by scanning laser Doppler vibrometry (SLDV), and reported in Fig. 6d. The clear drop in the transmission (blue line) can be seen as direct confirmation of the numerically predicted BG (the width of which is highlighted by the light blue rectangle in Fig. 6d). For the sake

of clarity, a numerical frequency response function (FRF) calculated through a finite element model using the same CAD file used for the manufacturing, is also plotted as the red line with circular markers, and superimposed on the measurements in Fig. 6d. Damping was added as an isotropic loss of $\eta = 0.025$. In this case, too, a good agreement is found (the slight discrepancy of some of the peaks may derive from a partial excitation of out-of-plane modes in the experiments, contrary to the numerical model where only in-plane modes are considered).

4. Conclusions and discussion

In conclusion, we have presented a new type of metamaterial made of a polymeric matrix with non self-similar cross-like holes at multiple scale levels to attenuate elastic waves. We have shown that the non self-similar hierarchy leads to multiple, broadband and highly attenuative bandgaps at various frequency scales, including the most challenging deep sub-wavelength regime. Numerical and experimental investigations have revealed that the opening of such bandgaps at different frequencies derive from the activation of multiple mechanisms. The activation of Bragg-, local resonance- and/or inertial amplification-driven mechanisms, as far as wave propagation at different frequencies is concerned, has been unequivocally identified by the behaviour of the imaginary part of the wavenumber. Finally, transmission experiments conducted in the lowest frequency regime, have shown a good agreement with the numerical predictions. In this work, we have limited the measurements to the lowest frequency regime involving the inertial amplification mechanism since the experimental verification of the opening of bandgaps in self-similar hierarchical elastic structures at higher frequencies is provided in Ref. [27].

This multi-mechanism based design approach leads to enriched dynamics at different scales, including the opening of additional bandgaps, the conservation of the existing ones down-shifted in frequency, as well as the possibility of preserving the global deformation mechanisms of the previous hierarchical levels despite the variation in mass-to-stiffness ratio.

The design proposed in this paper appears to be both robust and versatile for the conception of novel metamaterial structures, and can further be explored and optimized. For instance, the non self-similar hierarchical design offers additional opportunities compared to previous approaches, potentially leading to the simultaneous adaptation of geometrical features at different length scales for focused objectives. This can further be exploited by introducing more than two hierarchical
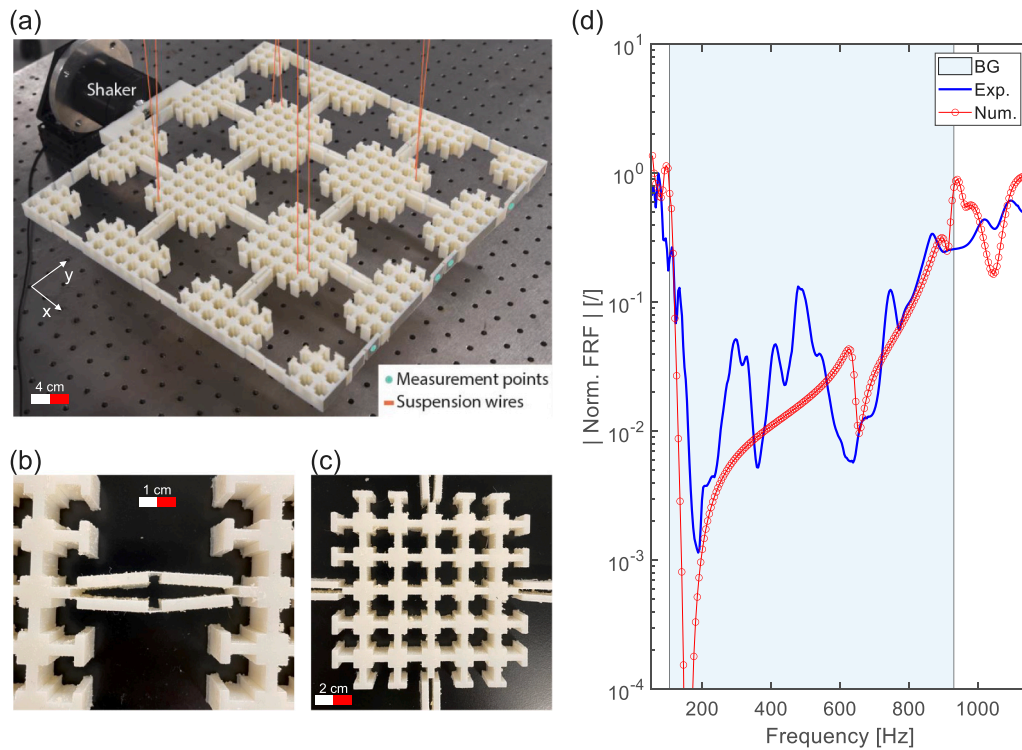
Fig. 6. Specimen, experimental setup and measured vs. calculated transmission spectra. (a) Finite hierarchical elastic metamaterial under investigation, with a cm scale, for reference. Suspension wires (in orange) hold the specimen in place during the measurements, reproducing free boundary conditions, also adopted in the numerical calculations. Elastic waves are excited through a shaker, visible in the top-left part of the picture, and solidly attached to the structure by means of a screw. Measurements are performed via a SLDV acquiring the x-displacement in correspondence of the cyan dots. (b, c) In-plane magnifications of the mass- and connecting-regions of the hierarchical elastic metamaterial, respectively. The smallest thickness of the printed specimen includes regions of 0.384 mm width (hinges of the mechanism of inertial amplification). (d) Measured (blue line) and calculated (red line with circular markers) transmission spectra of the specimen in the lowest frequency regime. The clear drop observed in the transmission approximately occurs in the 120–900 Hz frequency range, in good agreement with the numerically predicted bandgap (see left panel of Fig. 2a) reported as a light blue rectangle. The frequency response function (FRF) has been calculated as the ratio of the detected velocity (averaged over the four cyan points) and the imposed velocity at the shaker.

levels in the fabrication, as increasingly possible with last generation 3D printing and lithographic methods. Another possible direction of research is to exploit hierarchical design for simultaneous optimization of multiple properties, both quasistatic and dynamic (e.g., the design of lightweight structures providing both sound/vibration attenuation and high strength/toughness). The exploitation of hierarchical structures can thus provide unexplored possibilities of wave control for relatively direct application in different fields where vibrations play a crucial role, including civil, aerospace and mechanical engineering.

CRediT authorship contribution statement

M. Mazzotti: Performed the numerical calculations, Discussed results, Manuscript redaction. **A. Foehr:** Designed the structure, Discussed results. **O.R. Bilal:** Manufactured the structure and performed the experimental measurements, Discussed results, Manuscript redaction. **A. Bergamini:** Performed the numerical calculations, Discussed results, Manuscript redaction. **F. Bosia:** Conceived the work, Discussed results, Manuscript redaction. **C. Daraio:** Conceived the work, Designed the structure, Discussed results, Manuscript redaction. **N.M. Pugno:** Conceived the work, Discussed results, Manuscript redaction. **M. Miniaci:** Conceived the work, Designed the structure, Manufactured the structure and performed the experimental measurements, Performed the numerical calculations, Writing – original draft, Discussed results, Manuscript redaction.

Declaration of competing interest

The authors declare that they have no known competing financial interests or personal relationships that could have appeared to influence the work reported in this paper.

Data availability

Data will be made available on request.

Appendix A. Periodic structure made of solely the inertial amplification-based unit cell

In this Appendix, the periodic structure made of the *solely inertial amplification-based unit cell* is reported in Fig. A.1. It is obtained by repeating the unit cell reported in Fig. 1d infinitely in a linear array (in the x-direction).

Appendix B. Down-shift of the mid-frequency made of the periodic structure made by solely the inertial amplification-based unit cells

In this Appendix, we provide further insight on the frequency down-shift of the mid-frequency dispersion branch reported in green in Fig. 3a, as hierarchy is introduced. Fig. B.1 shows the evolution of the mode shapes (and of the dispersion bands) as we add cross-like holes such as those reported in Fig. 1c to the edges of the structure made
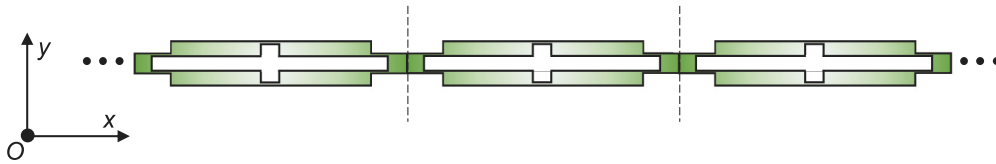
Fig. A.1. Periodic structure made by the solely inertial amplification-based unit cell infinitely duplicated in a linear array.
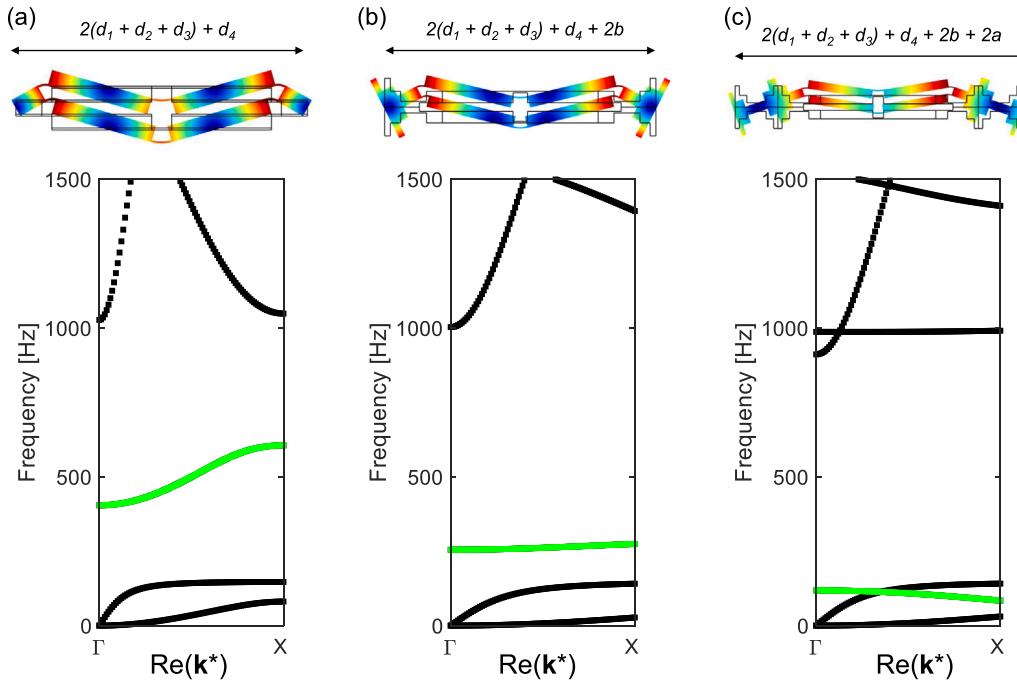

Fig. B.1. Down-shift of the mid-frequency mode of the structure solely made by the inertial amplification-based unit cells. As we add cross-like holes, such as those reported in Fig. 1c, to the edges of the structure solely made by the inertial amplification-based unit cells, we observe a slight alteration of the top bound of the upper bandgap and of the bottom bound of the lower bandgap of the structure solely made by the inertial amplification-based unit cells and a strong shift of the mid-frequency mode, highlighted in green. This is due to the fact that the virtual hinges of the mid-frequency deformation mode become more separated (assigning a selective compliance for this mode to the structure).

solely by the inertial amplification-based unit cells. Although the hierarchical structure and that made by solely the inertial amplification-based unit cells exhibit different stiffness and mass, as well as different types of connections between the periods, we can observe that: (1) Hierarchy only results in a slight alteration of the top bound of the upper bandgap and of the bottom bound of the lower bandgap of the structure made by solely the inertial amplification-based unit cells, whereas it strongly shifts the mid-frequency mode highlighted in green. This is due to the fact that the virtual hinges of the mid-frequency deformation mode become more separated (assigning a selective compliance for this mode to the structure). As a consequence, its frequency down-shifts.

(2) The specific arrangement of the inertial amplification mechanisms in the connecting regions of the hierarchical structure, allows the mechanism itself to take place almost unaltered (compare, for instance, M1 and M2 with m1 and m2 of Fig. 3b) as the wave propagates in both the structures.

References

[1] Meyers MA, McKittrick J, Chen P-Y. Structural biological materials: critical mechanics-materials connections. Science 2013;339(6121):773–9.

[2] Michel JA, Yunker PJ. Structural hierarchy confers error tolerance in biological materials. Proc Natl Acad Sci 2019;116(8):2875–80.

[3] Song J, Chen C, Zhu S, Zhu M, Dai J, Ray U, et al. Processing bulk natural wood into a high-performance structural material. Nature 2018;554(7691):224–8.

[4] Ji B, Gao H. Mechanical principles of biological nanocomposites. Annu Rev Mater Res 2010;40(1):77–100.

[5] Yarger JL, Cherry BR, Van Der Vaart A. Uncovering the structure–function relationship in spider silk. Nat Rev Mater 2018;3(3):1–11.

[6] Fernandes MC, Aizenberg J, Weaver JC, Bertoldi K. Mechanically robust lattices inspired by deep-sea glass sponges. Nature Mater 2021;20(2):237–41.

[7] Ambrosi D, Ben Amar M, Cyron CJ, DeSimone A, Goriely A, Humphrey JD, et al. Growth and remodelling of living tissues: perspectives, challenges and opportunities. J R Soc Interface 2019;16(157):20190233.

[8] Lakes R. Materials with structural hierarchy. Nature 1993;361(6412):511–5.

[9] Fratzl P, Weinkamer R. Nature's hierarchical materials. Prog Mater Sci 2007;52(8):1263–334.

[10] Matlack KH, Bauhofer A, Krödel S, Palermo A, Daraio C. Composite 3D-printed metastructures for low-frequency and broadband vibration absorption. Proc Natl Acad Sci 2016;113(30):8386–90.

[11] Bauer J, Hengsbach S, Tesari I, Schwaiger R, Kraft O. High-strength cellular ceramic composites with 3D microarchitecture. Proc Natl Acad Sci 2014;111(7):2453–8.

[12] Meza LR, Das S, Greer JR. Strong, lightweight, and recoverable three-dimensional ceramic nanolattices. Science 2014;345(6202):1322–6.

[13] Frenzel T, Kadic M, Wegener M. Three-dimensional mechanical metamaterials with a twist. Science 2017;358(6366):1072–4.

[14] Vigliotti A, Pasini D. Mechanical properties of hierarchical lattices. Mech Mater 2013;62:32–43.

[15] Deymier PA. Acoustic metamaterials and phononic crystals, Vol. 173. Springer Science & Business Media; 2013.

[16] Craster RV, Guenneau S. Acoustic metamaterials: negative refraction, imaging, lensing and cloaking, Vol. 166. Springer Science & Business Media; 2012.

[17] Kadic M, Milton GW, van Hecke M, Wegener M. 3D metamaterials. Nat Rev Phys 2019;1(3):198–210.

[18] Pham M-S, Liu C, Todd I, Lertthanasarn J. Damage-tolerant architected materials inspired by crystal microstructure. Nature 2019;565(7739):305–11.

[19] Meza LR, Zelhofer AJ, Clarke N, Mateos AJ, Kochmann DM, Greer JR. Resilient 3D hierarchical architected metamaterials. Proc Natl Acad Sci 2015;112(37):11502–7.

[20] Zhang X, Vyatskikh A, Gao H, Greer JR, Li X. Lightweight, flaw-tolerant, and ultrastrong nanoarchitected carbon. Proc Natl Acad Sci 2019;116(14):6665–72.

[21] Ritchie RO. The conflicts between strength and toughness. Nature Mater 2011;10(11):817–22.

[22] Lu H, Wang X, Chen T. Design and quasi-static responses of a hierarchical negative Poisson's ratio structure with three plateau stages and three-step deformation. Compos Struct 2022;291:115591.

[23] Yin S, Chen H, Li J, Yu T, Xu J. Effects of architecture level on mechanical properties of hierarchical lattice materials. Int J Mech Sci 2019;157:282–92.

[24] Wang Z, Zhou Y, Wang X, Wei K. Compression behavior of strut-reinforced hierarchical lattice—Experiment and simulation. Int J Mech Sci 2021;210:106749.

[25] Bosia F, Dal Poggetto VF, Gliozzi AS, Greco G, Lott M, Miniaci M, et al. Optimized structures for vibration attenuation and sound control in nature: A review. Matter 2022;5(10):3311–40.

[26] Zhang P, To AC. Broadband wave filtering of bioinspired hierarchical phononic crystal. Appl Phys Lett 2013;102(12):121910.

[27] Miniaci M, Krushynska A, Gliozzi AS, Kherraz N, Bosia F, Pugno NM. Design and fabrication of bioinspired hierarchical dissipative elastic metamaterials. Phys Rev Appl 2018;10:024012.

[28] Miniaci M, Kherraz N, Cröenne C, Mazzotti M, Morvaridi M, Gliozzi AS, et al. Hierarchical large-scale elastic metamaterials for passive seismic wave mitigation. EPJ Appl Metamaterials 2021;8:14.

[29] Jiang W, Yin G, Xie L, Yin M. Multifunctional 3D lattice metamaterials for vibration mitigation and energy absorption. Int J Mech Sci 2022;233:107678.

[30] Gao N, Wu JH, Jing L. Research on the band gaps of the two-dimensional sierpinski fractal phononic crystals. Modern Phys Lett B 2015;29(23):1550134.

[31] Gao N, Wu JH, Yu L. Large band gaps in two-dimensional phononic crystals with self-similarity structure. Internat J Modern Phys B 2015;29(04):1550017.

[32] Gao N, Hou H, Cheng B, Zhang R. A hollow inclusion self-similarity phononic crystal with an ultra-low-frequency bandgap. Internat J Modern Phys B 2018;32(02):1850005.

[33] Brillouin L. Wave propagation in periodic structures. McGraw-Hill Book Company, Inc.; 1946.

[34] Hussein MI, Leamy MJ, Ruzzene M. Dynamics of Phononic Materials and Structures: Historical Origins, Recent Progress, and Future Outlook. Appl Mech Rev 2014;66(4):040802.

[35] Li F-L, Wang Y-S, Zhang C. A BEM for band structure and elastic wave transmission analysis of 2D phononic crystals with different interface conditions. Int J Mech Sci 2018;144:110–7.

[36] Liu Z, Zhang X, Mao Y, Zhu Y, Yang Z, Chan C, et al. Locally resonant sonic materials. Science 2000;289(5485):1734–6.

[37] Yilmaz C, Hulbert GM, Kikuchi N. Phononic band gaps induced by inertial amplification in periodic media. Phys Rev B 2007;76(5):054309.

[38] Orta AH, Yilmaz C. Inertial amplification induced phononic band gaps generated by a compliant axial to rotary motion conversion mechanism. J Sound Vib 2019;439:329–43.

[39] Miniaci M, Mazzotti M, Amendola A, Fraternali F. Effect of prestress on phononic band gaps induced by inertial amplification. Int J Solids Struct 2021;216:156–66.

[40] Zangeneh-Nejad F, Alù A, Fleury R. Topological wave insulators: a review. Comptes Rendus Physique 2020;21(4–5):467–99.

[41] Nassar H, Yousefzadeh B, Fleury R, Ruzzene M, Alù A, Daraio C, et al. Nonreciprocity in acoustic and elastic materials. Nat Rev Mater 2020;5(9):667–85.

[42] Zhang S, Xia C, Fang N. Broadband acoustic cloak for ultrasound waves. Phys Rev Lett 2011;106:024301.

[43] Misseroni D, Colquitt DJ, Movchan AB, Movchan NV, Jones IS. Cymatics for the cloaking of flexural vibrations in a structured plate. Sci Rep 2016;6:23929.

[44] Pennec Y, Vasseur JO, Djafari-Rouhani B, Dobrzyński L, Deymier PA. Two-dimensional phononic crystals: Examples and applications. Surf Sci Rep 2010;65(8):229–91.

[45] Ma G, Sheng P. Acoustic metamaterials: From local resonances to broad horizons. Sci Adv 2016;2(2):e1501595.

[46] Aladwani A, Nouh M. Mechanics of metadamping in flexural dissipative metamaterials: analysis and design in frequency and time domains. Int J Mech Sci 2020;173:105459.

[47] Dal Poggetto VF, Serpa AL. Elastic wave band gaps in a three-dimensional periodic metamaterial using the plane wave expansion method. Int J Mech Sci 2020;184:105841.

[48] Lin Q, Zhou J, Wang K, Xu D, Wen G, Wang Q, et al. Low-frequency locally resonant band gap of the two-dimensional quasi-zero-stiffness metamaterials. Int J Mech Sci 2022;222:107230.

[49] Wu X, Wen Z, Jin Y, Rabczuk T, Zhuang X, Djafari-Rouhani B. Broad-band Rayleigh wave attenuation by gradient metamaterials. Int J Mech Sci 2021;205:106592.

[50] Krödel S, Delpero T, Bergamini A, Ermanni P, Kochmann DM. 3D auxetic microlattices with independently controllable acoustic band gaps and quasi-static elastic moduli. Adv Energy Mater 2014;16(4):357–63.

[51] Acar G, Yilmaz C. Experimental and numerical evidence for the existence of wide and deep phononic gaps induced by inertial amplification in two-dimensional solid structures. J Sound Vib 2013;332(24):6389–404.

[52] Bigoni D, Guenneau S, Movchan AB, Brun M. Elastic metamaterials with inertial locally resonant structures: Application to lensing and localization. Phys Rev B 2013;87(17):174303.

[53] Settimi V, Lepidi M, Bacigalupo A. Nonlinear dispersion properties of one-dimensional mechanical metamaterials with inertia amplification. Int J Mech Sci 2021;201:106461.

[54] Zeng Y, Cao L, Wan S, Guo T, Wang Y-F, Du Q-J, et al. Seismic metamaterials: Generating low-frequency bandgaps induced by inertial amplification. Int J Mech Sci 2022;221:107224.

[55] Banerjee A, Adhikari S, Hussein MI. Inertial amplification band-gap generation by coupling a levered mass with a locally resonant mass. Int J Mech Sci 2021;207:106630.

[56] Gasparetto VE, ElSayed MS. Multiscale optimization of specific elastic properties and microscopic frequency band-gaps of architectured microtruss lattice materials. Int J Mech Sci 2021;197:106320.

[57] Zhang X, Li Y, Wang Y, Jia Z, Luo Y. Narrow-band filter design of phononic crystals with periodic point defects via topology optimization. Int J Mech Sci 2021;212:106829.

[58] Chen Y, Wang L. Periodic co-continuous acoustic metamaterials with overlapping locally resonant and Bragg band gaps. Appl Phys Lett 2014;105(19):191907.

[59] Gao Y, Wang L, Sun W, Wu K, Hu H. Ultrawide bandgap in metamaterials via coupling of locally resonant and Bragg bandgaps. Acta Mech 2022;233(2):477–93.

[60] Still T, Cheng W, Retsch M, Sainidou R, Wang J, Jonas U, et al. Simultaneous occurrence of structure-induced and particle-resonance-induced phononic gaps in colloidal films. Phys Rev Lett 2008;100:194301.

[61] Yuan B, Humphrey VF, Wen J, Wen X. On the coupling of resonance and Bragg scattering effects in three-dimensional locally resonant sonic materials. Ultrasonics 2013;53(7):1332–43.

[62] Assouar MB, Sun J-H, Lin F-S, Hsu J-C. Hybrid phononic crystal plates for lowering and widening acoustic band gaps. Ultrasonics 2014;54(8):2159–64.

[63] Krushynska A, Miniaci M, Bosia F, Pugno N. Coupling local resonance with Bragg band gaps in single-phase mechanical metamaterials. Extreme Mech Lett 2017;12:30–6.

[64] Jiang W, Yin M, Liao Q, Xie L, Yin G. Three-dimensional single-phase elastic metamaterial for low-frequency and broadband vibration mitigation. Int J Mech Sci 2021;190:106023.

[65] Xiao Y, Mace BR, Wen J, Wen X. Formation and coupling of band gaps in a locally resonant elastic system comprising a string with attached resonators. Phys Lett A 2011;375(12):1485–91.

[66] Tian X, Chen W, Gao R, Liu S. Merging bragg and local resonance bandgaps in perforated elastic metamaterials with embedded spiral holes. J Sound Vib 2021;500:116036.

[67] Li Y, Xiao Y, Guo J, Zhu Z, Wen J. Single-phase metabeam for three-directional broadband vibration suppression. Int J Mech Sci 2022;107683.

[68] Frandsen NM, Bilal OR, Jensen JS, Hussein MI. Inertial amplification of continuous structures: Large band gaps from small masses. J Appl Phys 2016;119(12):124902.

[69] Mi Y, Yu X. Sound transmission of acoustic metamaterial beams with periodic inertial amplification mechanisms. J Sound Vib 2021;499:116009.

[70] Miniaci M, Marzani A, Testoni N, De Marchi L. Complete band gaps in a polyvinyl chloride (PVC) phononic plate with cross-like holes: numerical design and experimental verification. Ultrasonics 2015;56:251–9.

[71] Miniaci M, Mazzotti M, Radzieński M, Kherraz N, Kudela P, Ostachowicz W, et al. Experimental observation of a large low-frequency band gap in a polymer waveguide. Front Mater 2018;5:8.

[72] Lim QJ, Wang P, Koh SJA, Khoo EH, Bertoldi K. Wave propagation in fractal-inspired self-similar beam lattices. Appl Phys Lett 2015;107(22):221911.

[73] Mousanezhad D, Babaee S, Ghosh R, Mahdi E, Bertoldi K, Vaziri A. Honeycomb phononic crystals with self-similar hierarchy. Phys Rev B 2015;92:104304.

[74] Chen Y, Wang L. Harnessing structural hierarchy to design stiff and lightweight phononic crystals. Extreme Mech Lett 2016;9:91–6.

[75] Maldovan M. Sound and heat revolutions in phononics. Nature 2013;503(7475):209–17.

[76] Minelli A, Fusco G, Sartori S. Self-similarity in biological classifications. BioSystems 1991;26(2):89–97.

[77] Weibel ER. Fractal geometry: a design principle for living organisms. Am J Physiol-Lung Cell Mol Physiol 1991;261(6):L361–9.

[78] Abhirami A, Anup S. Mechanical properties of unidirectional bio-inspired composites with two non-self-similar hierarchical structures. Mech Mater 2021;163:104082.

[79] Peters EN. Plastics: thermoplastics, thermosets, and elastomers. Wiley-Interscience, New York; 2002.

[80] Collet M, Ouisse M, Ruzzene M, Ichchou M. Floquet–Bloch decomposition for the computation of dispersion of two-dimensional periodic, damped mechanical systems. Int J Solids Struct 2011;48(20):2837–48.

[81] Mazzotti M, Miniaci M, Bartoli I. Band structure analysis of leaky Bloch waves in 2D phononic crystal plates. Ultrasonics 2017;74:140–3.